17th World Conference on Earthquake Engineering, 17WCEE
Sendai, Japan - September 13th to 18th 2020

EXPERIMENTAL AND NUMERICAL STUDY OF A STAINLESS STEEL TUBE-IN-TUBE DAMPER FOR PASSIVE ENERGY DISSIPATION

D. Escolano-Margarit(1), G. González-Sanz(2), A. Benavent-Climent(3)

(1) *Lecturer, Universidad Politécnica de Madrid, d.escolano@upm.es*
(2) *PhD. student, Universidad Politécnica de Madrid, guillermo.gonzalez.sanz@upm.es*
(3) *Professor, Universidad Politécnica de Madrid, amadeo.benavent@upm.es*

Abstract

Passive control systems such as energy dissipation devices, are a cost-effective and innovative technology to control the vibration of structures. When included in the main structure, they can improve the overall performance of the building, reducing the seismic response in terms of displacements, and more importantly attracting most of the energy input by the ground motion. The simplest amongst them are metallic dampers. This study proposes a Stainless Steel Tube-in-Tube Damper (SS-TTD) which source of energy dissipation is the plastic deformations of slit-type plates. It constructs through the assemblage of two standard rectangular tubes with a telescopic configuration. All faces of the outer tube are regularly slit transversally to its longitudinal axis, forming strips which are the dissipative part of the dampers. When the brace is subjected to axial force, the relative displacements between the tubes impose a double curvature deformation on the struts which behave as a series of fixed-ended beams, dissipating energy through flexural yielding. The performance of three identical SS-TTDs in terms of hysteretic behaviour, ductility and ultimate energy dissipation capacity, was investigated trough dynamic shake table and quasi-static cyclic tests. The ultimate energy dissipation capacity has been studied with a path-dependent damage model based on the decomposition of the hysteretic curves into the called skeleton and Bauschinger parts. The results show that the proposed SS-TTD exhibits a stable hysteretic behaviour with large ductility and large ultimate energy dissipation capacity. Finally, a numerical model is proposed to characterize the hysteretic behavior.

Keywords: Metallic damper, Stainless steel, Shake table test, Cyclic loading, Energy dissipation.

1. Introduction

The traditional approach of ensuring life safety against earthquakes has been long proven invalid, especially after the Kobe (1995) and Northridge (1994) earthquakes. After these, it was found that the large economic losses after an earthquake were unaffordable and are also to be considered in aseismic design of building and infrastructures. In this sense an important research effort has been done recently to the development of innovative systems to control the dynamic response of structures. Among the passive control systems, the displacement-dependent energy dissipation devices (EDD/Dampers), are a cost-effective technology widely used in seismic prone areas. Including EDD's within the main gravity load resistant structure, improves the overall dynamic performance of the building, reducing displacements, forces and accelerations, and more importantly dissipating most of the energy input. Therefore, damage concentrates in specific well engineered elements (the EDDs), which are easy to inspect, repair and/or replace after an earthquake, avoiding or reducing drastically the damage on the main structure and minimizing disruption on the building use. Displacement-dependent dampers use different mechanisms to dissipate energy: metal yielding, metal phase transformation, friction, sliding etc. The most straightforward among all are the metallic dampers. They built on well-known and reliable materials with stable hysteretic behaviour and resistance against ambient temperature. For that reason, a large number of metallic dampers have been developed since the early 1970s. A state-of-the-art review on metallic dampers can be found in [1]. An interesting EDD type which has drawn attention lately are the slit dampers (SD) which are built slitting steel plates transversally to its longitudinal axis, forming stips. The yielding mechanism works by in-plane bending of the strips as shown in Fig. 1.

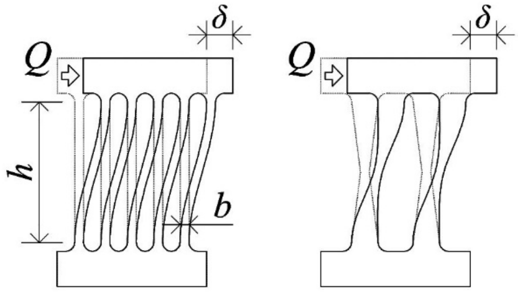

Fig. 1 – Metallic dampers. a) slit-type damper b) honeycomb damper

Several studies investigating slit dampers have been carried out over the last decade [2-6]. This study proposes an upgraded Stainless-steel Tube in Tube damper (SS-TTD). Its performance in terms of hysteretic behaviour, ductility and ultimate energy dissipation capacity was investigated trough dynamic shake table test and quasi-static cyclic tests. A comparison with other dampers proposed in the literature is also presented. Finally, two numerical models are investigated to characterize the hysteretic behaviour under arbitrary cyclic loading.

2. Proposed seismic damper

The proposed seismic damper builds on previous studies of brace-type seismic dampers based on yielding the walls of hollow structural sections [7]. It constructs trough the assemblage of two standardize rectangular tubes with a telescopic configuration (Fig. 2), that are connected to the main structure through auxiliary linear elements that form a braced member. The outer tube is regularly slit transversally to its longitudinal axis, forming strips. The inner tube welds to the outer tube in discrete points along the overlapping length, increasing the buckling capacity. These strips conform the energy dissipating part of the damper. When subjected to axial forces the relative displacements between the tubes, impose a double curvature deformation on the strips which behave as a series of fixed-ended beams.

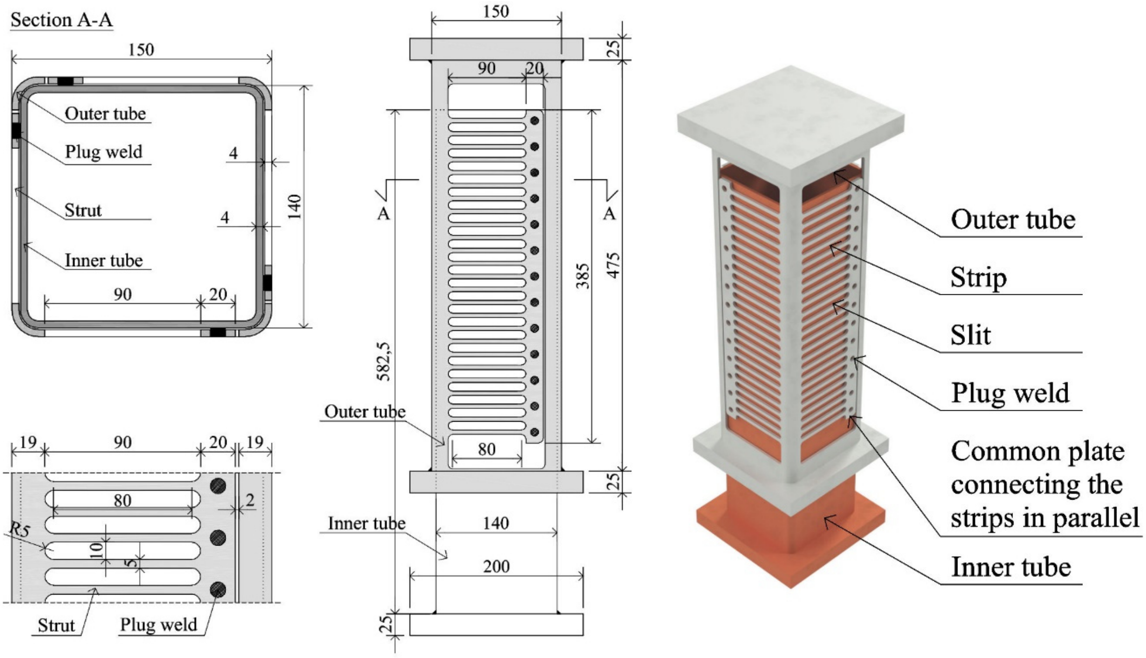

Fig. 2 – Proposed Tube-in-Tube Damper.

3. Experimental investigation

The experimental testing of the proposed damper was focused on the hysteretic behaviour and the ultimate energy dissipation capacity. Two different tests were carried out to three identical specimens: i) dynamic shake table tests; and ii) quasi-static cyclic tests. Fig. 2 shows the dimensions and geometry of the specimen. The squared hollow tubes used to construct the specimen were #150.4mm and #140.4mm (#width.thickness) for the outer and inner tubes, respectively. The steel between the slits leave a total of 100 strips in the outer tube (25 per face) with dimensions of b=5mm, h=80mm, t=4mm and a radius of the ends of r=5mm. The material used for building the specimens up was stainless steel, grade 1.4301 (304-L AISI).

3.1 Material testing

The mechanical properties were obtained from standard coupon tests, following the indications of ISO 6892-1:2016 [8]. The strain rate effect was studied by testing the material under different strain rates, 0.003 mm/mm/s for quasi-static and 0.115mm/mm/s for dynamic loading. The same protocol was repeated twice. The mean values and the standard deviation obtained from the test are summarized in Table 1. In the table, $\sigma_{0.2\%}$, is a common parameter used for stainless steel and it represents the stress at 0.2% strain, σ_u and ε_u are the ultimate stress and strain, respectively. In this study, several parameters are defined for convenience: (σ_y, ε_y) yielding stress and strain at the limit of proportionality; and (σ_b, ε_b) stress and strain at the end of the smooth transition branch from elastic to inelastic range. The values of these parameters are obtained by an idealization of the stress-stain curve obtained from tests as follows: (i) an initial linear-elastic branch with a slope equal to the modulus of elasticity E until the proportionality limit (σ_y, ε_y); (ii) a transition linear branch from (σ_y, ε_y) to (σ_b, ε_b); (iii) a third linear branch that fits the inelastic part from (σ_b, ε_b) to (σ_u, ε_u). The transition branch was determined so as the area under the trilinear approximation and the real curve was the same. For all the tests, the modulus of elasticity was identical: E=200000MPa.

Table 1 – Mechanical properties of the stainless steel at different strain rates

Strain rate mm/mm/s	$\sigma_{0.2\%}$ MPa	σ_u MPa	σ_y MPa	σ_b MPa	ε_y %	ε_b %	ε_u %
0.003 (static)	377±15	604±30	250±5	405±15	0.12±0.05	0.40±0.01	46±1
0.115 (dynamic)	529±6	709±16	400±10	560±15	0.20±0.01	0.57±0.02	44±2

3.2 Shake table Dynamic tests

The hysteretic behaviour of the damper under realistic earthquake loadings was studied by shake table tests at the Laboratory of Structural Dynamics of the University of Granada (Spain). The whole specimen tested comprises a portion of a reinforced concrete structure consisting of waffle-flat plates supported on isolated columns. The specimen was designed according to Spanish construction codes [9, 10] for gravity loads only. A set of three SS-TTDs per floor (six in total) were used as diagonal bars for resisting lateral loads. Fig. 3 shows the main structure with the SS-TTDs installed. The scaled factor used for the length of the elements was λ_L=2/5. More details of a similar specimen are described in [11].

A 3x3m^2 shake table was used to perform bidirectional seismic tests. The instrumentation and set-up in the whole structure comprises displacement transducers (LVDTs), accelerometers and more than 400 strain gauges. The relative axial displacements on the SS-TTDs were measured with a pair of LVDTs in each damper. For obtaining the axial loads, a set of six strain gauges were put in auxiliary square hollow sections (#80.4mm) that connect the SS-TTDs to the main structure.

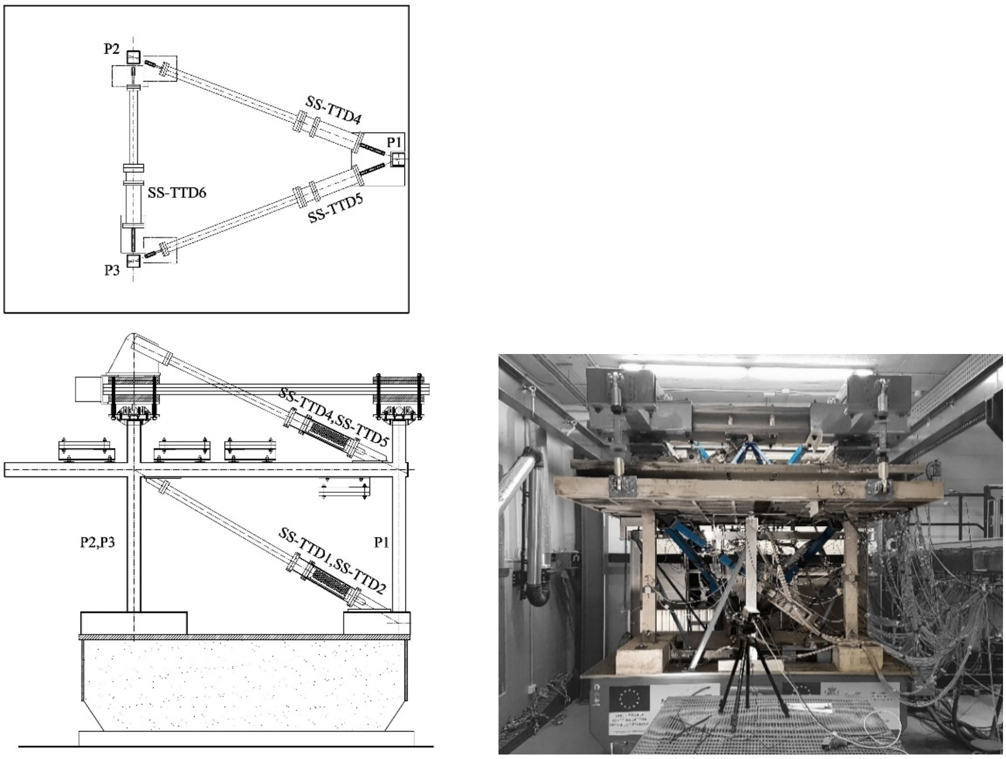

Fig. 3 – General overview of the test specimen in the shake table.

A near fault ground motion recorded at Bar-Skupstina Opstine (Montenegro, 1979) was used to subject the specimen to an increasing intensity series of shake table tests. The recording was scaled in time consistently with the specimen scale factors. In each test, the two horizontal components of the ground motions were applied simultaneously. Different levels of intensity were represented by increasing the ground motion amplitude in consecutive tests, as defined in [11].

The emphasis of this research is placed on the response of the three SS-TTDs of the upper floor (namely SS-TTD4, SS-TTD5, SS-TTD6). The hysteretic behaviour (axial force versus axial displacement) along the test series is represented in Fig. 4. The SS-TTDs endured large plastic deformations but did not fail during the tests. It is worth noting that the main structure remained basically elastic at the end of the tests.

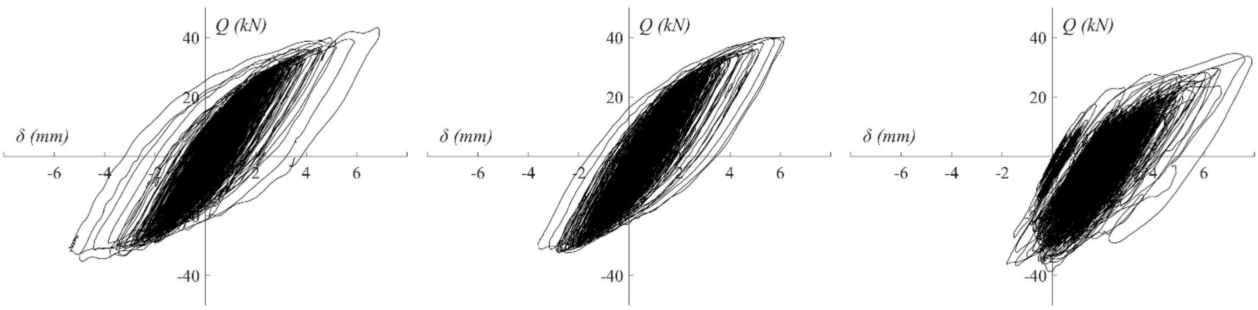

Fig. 4 – Q-δ curves obtained from the shake table tests: (a) SS-TTD4, (b) SS-TTD5, (c) SS-TTD6.

3.3 Quasi-static cyclic tests

With the aim of characterizing the ultimate energy dissipation capacity and deformation, the three SS-TTDs used in the shake table tests were subjected to different cyclic loadings until failure with an uniaxial universal testing machine. Each specimen was fixed in its ends to a rigid base and to the actuator respectively. The tests were performed in quasi-static conditions with a cyclic rate of 0.02Hz under displacement control. The force was recorded by the actuator load cell and the relative displacement was measured and controlled by two LVDTs installed in the axial direction between the tubes. The complete set-up is shown in Fig. 5.

Three different cyclic displacements histories were applied to the SS-TTDs. An initial displacement of 10mm in positive direction followed by constant amplitude cycles of 5 times the yield displacement, δ_{yST}, were applied to the specimen SS-TTD4. For the specimens SS-TTD5 and SS-TTD6 a sequence of incremental amplitude cycles was selected, following the indications of the ATC for structural elements [12]. The increment of amplitude $\Delta\delta$, was $\Delta\delta/\delta_{yST}$=1 in both cases, but the difference was the number of cycles repetition n_c. For the SS-TTD5 n_c =10 while for the SS-TTD6 n_c =4. The failure was assumed to occur when the maximum force dropped below 20% of the one obtained in previous cycles.

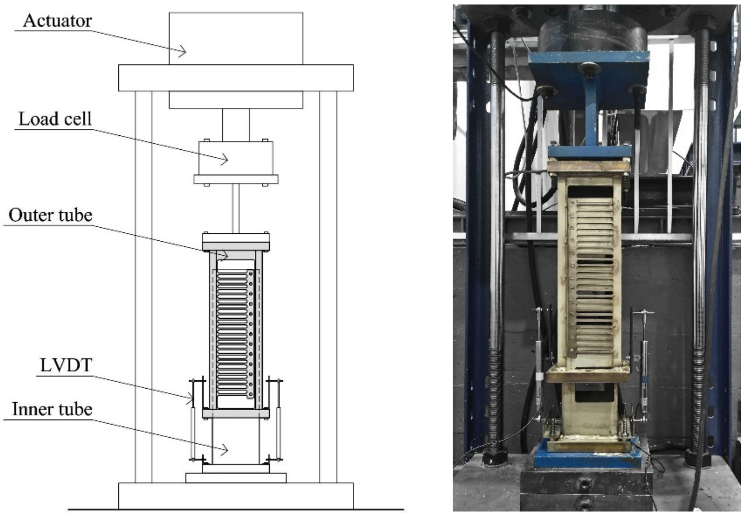

Fig. 5 – Experimental set-up used during the cycling tests.

Fig. 6 shows with solid lines the hysteresis loops prior to the failure point, as described in next section. Dotted lines indicate the *Q-δ* curves after failure. Failure was assumed to occur when, under increasing forced displacements, the restoring force drop below 80% of the maximum force attained in previous cycles.

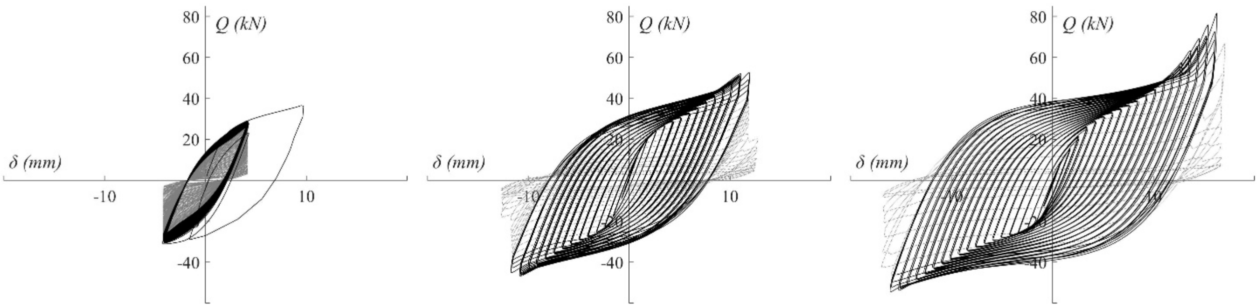

Fig. 6 – *Q-δ* curves obtained from the quasi-static cyclic tests: (a) SS-TTD4, (b) SS-TTD5, (c) SS-TTD6.

4. Results and discussion

The seismic performance of the SS-TTD is fully characterized with the load-displacement relationship (i.e. *Q-δ* hysteretic loops) in Fig. 7. In order to merge the quasi-static and dynamic loading the strain rate effect [13,14,15] needs to be accounted for. Therefore, the curves obtained from the dynamic shake table tests and those obtained from the quasi-static cyclic tests were normalized by their respective yielding force (Q_y) and yielding displacement (δ_y). Q_y and δ_y were obtained from analytical equations in the literature [7], using the material properties obtained from the dynamic and quasi-static tensile tests at different strain rates (Table 1). The theoretical values calculated for the proposed SS-TTD are: Q_{yST}=15.5kN, Q_{BST}=25.14kN, δ_{yST}=1.08mm for the quasi-static strain rate, and Q_{yDYN}=24.83kN, Q_{BDYN}=34.76kN, δ_{yDYN}=1.73mm for the dynamic strain rate respectively.

As can be observed in the shape of the hysteresis loops, the SS-TTD has a very stable behaviour with loop shape close to a rectangle; the strength or stiffness degradation between cycles is negligible. Second order effects due to geometric nonlinearity of the steel strips caused sudden peaks of force at ductility levels above 12. This level of ductility is larger than the maximum ductility typically allowed in frame structures to avoid or limit the damage.

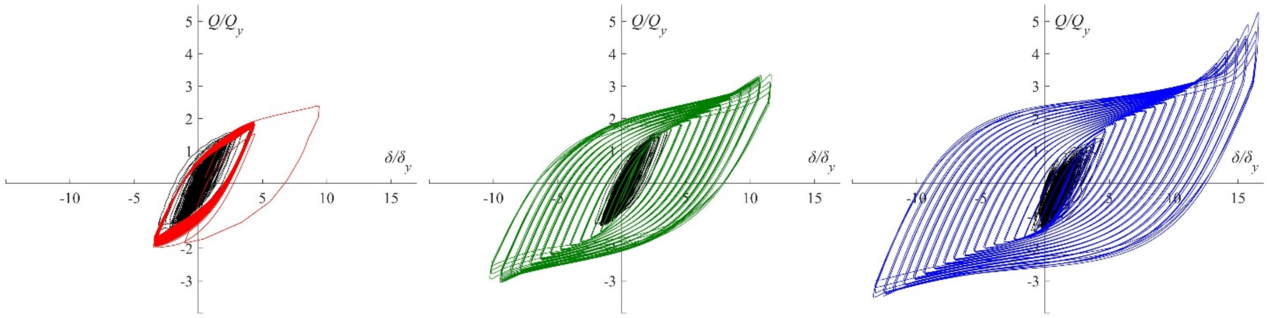

Fig. 7 – Total normalized Q-δ curves of the tested specimens: (a) SS-TTD4, (b) SS-TTD5, (c) SS-TTD6.

4.1 Ultimate energy dissipation capacity

Several studies in the literature [16,17,18] pointed out that the loading pattern applied to a metallic damper affects its ultimate energy dissipation capacity. This dependency can be represented by splitting the total energy dissipated by the damper into two parts, the skeleton part and the Bauschinger part as explained in detail in [7]. From the results of the decomposition of the Q-δ curve, the total plastic strain energy dissipated by the damping device in each domain of loading until failure on the skeleton and the Bauschinger parts can be expressed non-dimensionally as follows:

$$
{}_S\eta^+ = \frac{{}_SW_u^+}{Q_y\delta_y}; \quad {}_S\eta^- = \frac{{}_SW_u^-}{Q_y\delta_y}; \quad {}_B\eta^+ = \frac{{}_BW_u^+}{Q_y\delta_y};
$$
$$
{}_B\eta^- = \frac{{}_BW_u^-}{Q_y\delta_y}; \quad {}_{ep}\eta^+ = \frac{{}_S\delta_u^+}{\delta_y}; \quad {}_{ep}\eta^- = \frac{{}_S\delta_u^-}{\delta_y}; \qquad (1)
$$

Based on the above the following ratios are defined as in [14]: The apparent cumulative plastic deformation ratio on the skeleton part, ${}_{ep}\eta$; the cumulative energy ratio on the skeleton part, ${}_S\eta$; the cumulative energy ratio on the Bauschinger part ${}_B\eta$; and the total cumulative energy ratio, η, which in turn is a non-dimensional form the total energy dissipated by the damper until failure $W_u = {}_SW_u^+ + {}_SW_u^- + {}_BW_u^+ + {}_BW_u^-$.

$$
{}_S\eta = |{}_S\eta^+| + |{}_S\eta^-|; \quad {}_B\eta = |{}_B\eta^+| + |{}_B\eta^-|; \quad {}_{ep}\eta = |{}_{ep}\eta^+| + |{}_{ep}\eta^-|; \quad \eta = {}_S\eta + {}_B\eta \qquad (4)
$$

The SS-TTD Q-δ curves from Fig 7 were decomposed into the skeleton and Bauschinger parts. Table 2 summarises the ratios defined in Eqs. (1) and (2). Fig. 8 shows the curves and the idealized trilinear skeleton curve which normalized plastic stiffness are k_{p1} = 1/2.5 and k_{p2} = 1/14.

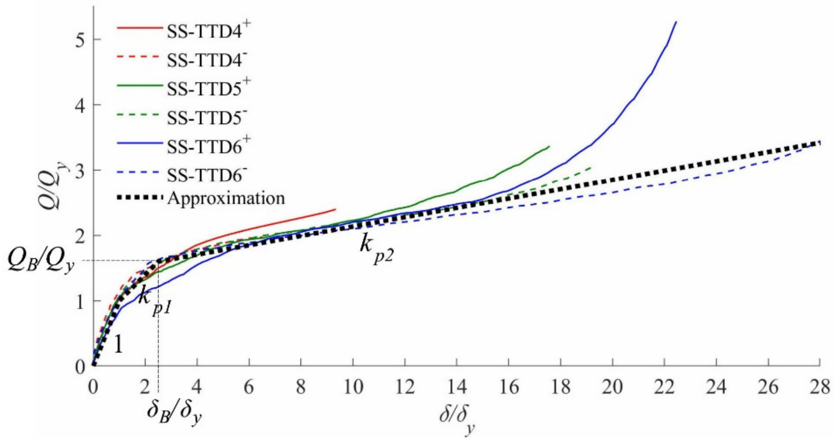

Fig. 8 – Skeleton curves

Table 2 – Loading protocol of the specimens and ultimate energy dissipation capacity

Specimen	${}_{ep}\eta^{+}$ - ${}_{ep}\eta^{-}$	${}_{S}\eta^{+}$ - ${}_{S}\eta^{-}$	${}_{B}\eta^{+}$ - ${}_{B}\eta^{-}$	η^{+} - η^{-}	η	μ_{CUM}	${}_{B}\eta$ / ${}_{S}\eta$
SS-TTD5	17.6 - 19.3	37 - 41	1643 - 1611	1680 - 1652	3332	1912	41.7
SS-TTD6	22.5 - 28.4	54 - 66	1700 - 1633	1754 - 1699	3453	1728	27.8
SS-TTD4	9.3 - 6.5	16 - 10	1884 - 1856	1900 - 1866	3766	2707	143.8

The results in Table 2 show a dependency of η to the loading pattern. Therefore, the energy dissipated on the skeleton and the Bauschinger part was analysed independently. Fig. 9 (a, b) plot the relation between ${}_{ep}\eta$ *versus* ${}_{B}\eta$ and ${}_{ep}\eta$ *versus* ${}_{S}\eta$ respectively. Likewise, the ultimate energy dissipation capacity in the Bauschingher part (Fig. 9a), skeleton part (Fig.9b) and total (Fig.9c) predicted as explained in [16] was plotted with black solid line, showing a very good agreement with the experimental results.

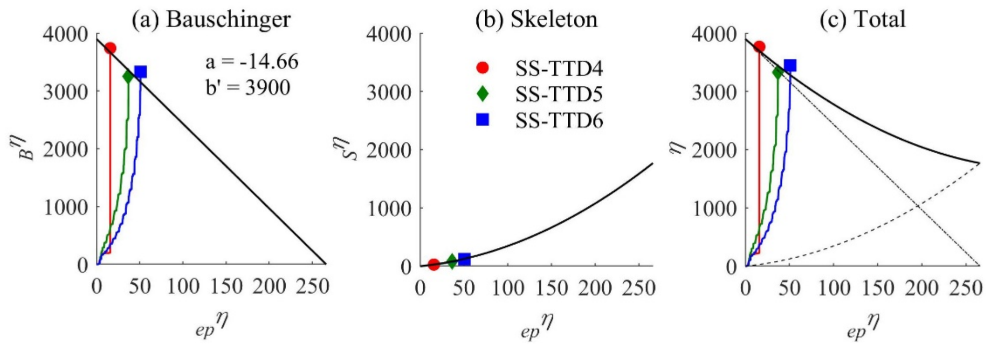

Fig. 9. – Ultimate energy dissipation capacity: (a) Bauschinger part, (b) Skeleton part, (c) Total

5. Numerical characterization

The shape of the hysteretic loops of the SS-TTD under arbitrarily applied cyclic loads can be predicted with a simple polynomial model that is founded on the decomposition of the *Q-δ* curves in the skeleton and Bauschinger parts. Detailed explanation of the model can be found in [7]. The approximated trilinear curve shown with bold dot lines in Fig. 8 is adopted for the skeleton curve. The shape of the Bauschinger parts is modelled with two segments [7] that are defined by two parameters, α and β, that are obtained from the tests. All the necessary parameters and values to build the model up are resumed in Table 3.

Table 3 – Normalized parameters defining polynomial numerical model

Parameter	Q_y	δ_y	τ_B	k_{p1}	k_{p2}	α	β
Algorithm	1	1	1.6	0.4	1/14	0.40	0.35

With the aim of assessing the prediction given by the polygonal model, the displacement history from the experiments were imposed numerically. The experimental results and the prediction provided by the polygonal model for the three specimens are compared in Fig. 10.

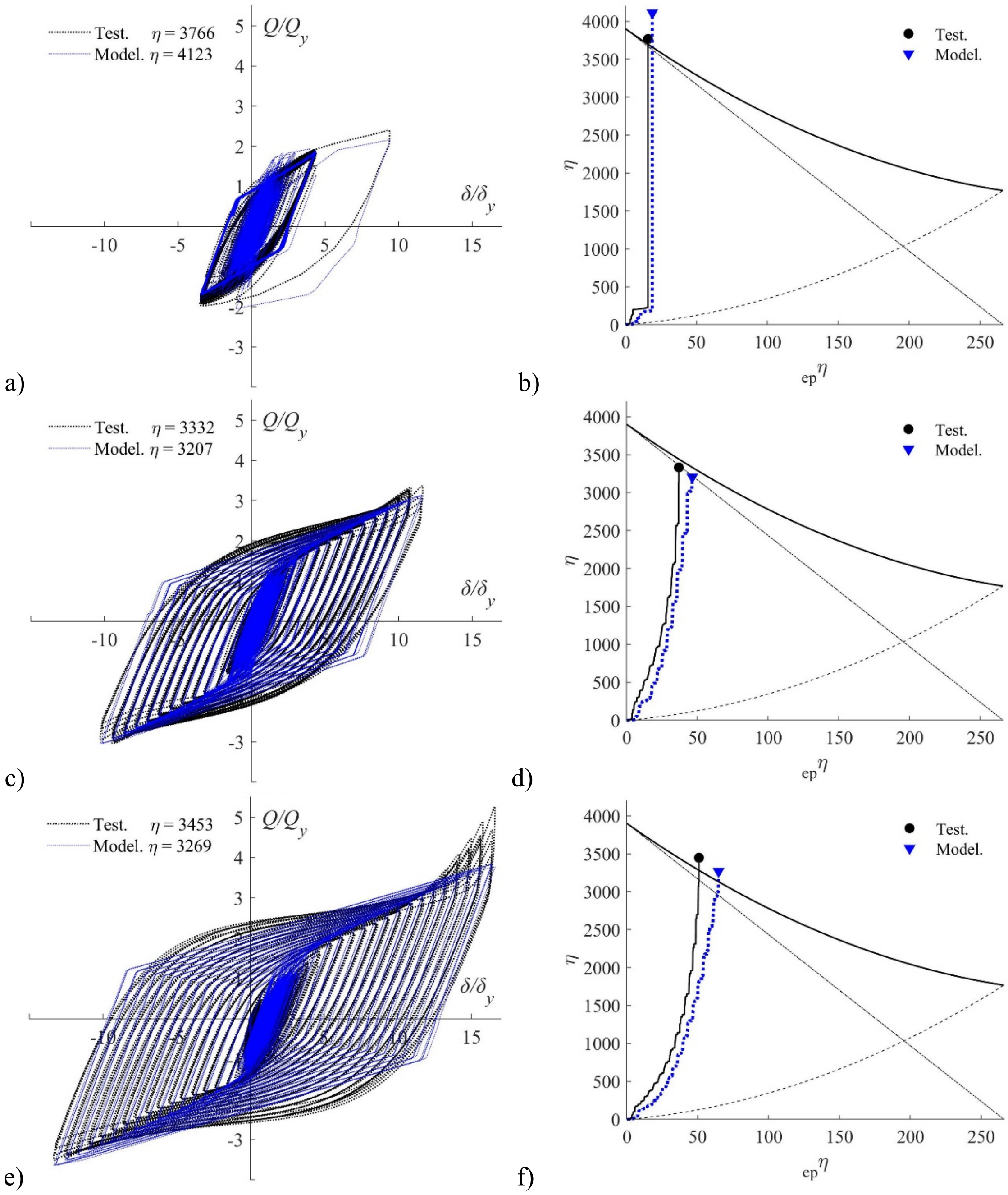

Fig. 10 Tests versus numerical models for specimens SS-TTD4 (a,b), SS-TTD5 (c,d) and SS-TTD6 (e,f)

Figure 10 (left) compares the hysteresis loops. Figure 10 (right) compares the "energy dissipation path" [7] followed by each test specimen (solid line), and by the numerical model (blue dot line) until failure. It can be seen that the shape of the hysteresis loops, the "energy dissipation paths" and the point of failure (circle and triangle symbols) are in good agreement. Moe precisely, the point of failure predicted by the numerical model is very close to that obtained from the tests, with errors below 10%. The strain hardening that comes up in SS-TTD6 with large ductility values is not captured with the polynomial model, but the impact on the overall response is negligible.

6. Conclusions

This paper studied a Stain Steel Tube-in-Tube Damper (SS-TTD) which source of energy dissipation is the plastic deformation of slit-type plates. The seismic behaviour of three SS-TTD specimens was assessed experimentally trough two different types of tests: shake table dynamic test and quasi-static cyclic loading . From the experimental results the following conclusions can be drawn:

- The SS-TTD shows a stable hysteretic behaviour dissipating large amounts of energy per cycle.
- The SS-TTD presents a ductility around 12-15 before large strain hardening occurs due to geometric nonlinearity.
- The ultimate energy dissipation capacity has also been studied with a path-dependent damage model based on the decomposition of the hysteretic curves into the so-called skeleton and Bauschinger parts.

A numerical model is proposed to predict the hysteretic response and the point of failure of the proposed SS-TTD. This path dependent model is based on the shape of the skeleton part and the shape of each segment of the Bauschinger part. The prediction provided by the numerical model is compared with the experimental results and a very good agreement is founded.

7. Acknowledgements

This research was supported by the Spanish Ministry of Economy and Competitivity, research grant MEC BIA2017 88814 R and received funds from the European Union (Fonds Européen de Dévelopment Régional).

9. References

[1] Javanmardi, A., Ibrahim, Z., Ghaedi, K., Benisi Ghadim, H., & Hanif, M. U. (2019). State-of-the-art review of metallic dampers: Testing, development and implementation. *Archives of Computational Methods in Engineering,* doi:10.1007/s11831-019-09329-9

[2] Chan, R. W. K., & Albermani, F. (2008). Experimental study of steel slit damper for passive energy dissipation. *Engineering Structures, 30*(4), 1058-1066. doi:10.1016/j.engstruct.2007.07.005

[3] Teruna, D. R., Majid, T. A., & Budiono, B. (2015). Experimental study of hysteretic steel damper for energy dissipation capacity. *Advances in Civil Engineering,* , 631726. doi:10.1155/2015/631726

[4] Lee, C., Ju, Y. K., Min, J., Lho, S., & Kim, S. (2015). Non-uniform steel strip dampers subjected to cyclic loadings. *Engineering Structures, 99*, 192-204. doi:10.1016/j.engstruct.2015.04.052

[5] Lee, C., Lho, S., Kim, D., Oh, J., & Ju, Y. K. (2016). Hourglass-shaped strip damper subjected to monotonic and cyclic loadings. *Engineering Structures, 119*, 122-134. doi:10.1016/j.engstruct.2016.04.019

[6] Amiri, H. A., Najafabadi, E. P., & Estekanchi, H. E. (2018). Experimental and analytical study of block slit damper. *Journal of Constructional Steel Research, 141*, 167-178. doi:10.1016/j.jcsr.2017.11.006

[7] Benavent-Climent, A. (2010). A brace-type seismic damper based on yielding the walls of hollow structural sections. *Engineering Structures, 32*(4), 1113-1122. doi:10.1016/j.engstruct.2009.12.037

[8] ISO 6892-1:2016. Metallic materials. Tensile testing. Part 1: Method of test at room temperature.

[9] Ministerio de Fomento. Instrucción de Hormigón Estructural (2008). *EHE-08*. Madrid: Centro Publicaciones.

[10] Ministerio de Fomento. Norma de Construcción Sismorresistente (2003). *Parte General y Edificación (NSCE-02)*. Madrid: Centro Publicaciones.

[11] Benavent-Climent, A., Gale-Lamuela, D., & Donaire-Avila, J. (2019). Energy capacity and seismic performance of RC waffle-flat plate structures under two components of far-field ground motions: Shake table tests. *Earthquake Engineering & Structural Dynamics, 48*(8), 949-969. doi:10.1002/eqe.3161

[12] ATC. Guidelines for Cyclic Seismicl Testing of Components of Steel Structures (1992). Applyied Technology Council, Redwood City, CA, USA.

[13] Cadoni, E., Fenu, L., & Forni, D. (2012). Strain rate behaviour in tension of austenitic stainless steel used for reinforcing bars. *Construction and Building Materials, 35*, 399-407. doi:10.1016/j.conbuildmat.2012.04.081

[14] Lichtenfeld, J. A., Mataya, M. C., & Van Tyne, C. J. (2006). Effect of strain rate on stress-strain behavior of alloy 309 and 304L austenitic stainless steel. *Metallurgical and Materials Transactions A-Physical Metallurgy and Materials Science, 37A*(1), 147-161. doi:10.1007/s11661-006-0160-5

[15] Lee, W. S., Lin, C. F., & Chen, B. T. (2005). Tensile properties and microstructural aspects of 304L stainless steel weldments as a function of strain rate and temperature. *Proceedings of the Institution of Mechanical Engineers Part C-Journal of Mechanical Engineering Science, 219*(5), 439-451. doi:10.1243/095440605X17045

[16] Benavent-Climent, A. (2007). An energy-based damage model for seismic response of steel structures. *Earthquake Engineering & Structural Dynamics, 36*(8), 1049-1064. doi:10.1002/eqe.671

[17] Kato B, Akiyama H, Yamanouchi H. (1973). Predictable properties of structural steels subjected to incremental cyclic loading. In: *IABSE symposium on resistance and ultimate deformability of structures acted on by well-defined loads*, p. 119-24.

[18] Jiao, Y., Shimada, Y., Kishiki, S., & Yamada, S. (2009). In Mazzolani, FM Ricles, JM Sause,R. (Ed.), *Study of energy dissipation capacity of steel beams under cyclic loading*. Boca raton; 6000 broken sound parkway nw, ste 300, boca raton, fl 33487-2742 usa: crc press-taylor & francis group.

